Journal of Physiology (1995), **489.2**, *pp.*473–488

Kinetic characterization of the voltage-gated currents possessed by *Xenopus* embryo spinal neurons

Nicholas Dale*

School of Biological Sciences, University of Bristol, Woodland Road, Bristol BS8 1UG, UK

1. Using the whole-cell patch clamp technique, the voltage-gated currents of neurons acutely isolated from the *Xenopus* embryo spinal cord were studied.

2. The spinal neurons possessed a very fast Na^+ current, which activated with time constants that ranged from 0·1 to 0·25 ms. It was also subject to rapid inactivation with time constants ranging from 0·3 to 8 ms. This current could only be fitted with Hodgkin–Huxley equations once the rapid inactivation that occurs by the time of the peak current had been taken into account.

3. *Xenopus* embryo neurons also possessed a mixture of kinetically similar Ca^{2+} currents, which activated with time constants that ranged from 0·3 to 0·8 ms. Sometimes the Ca^{2+} currents showed very slow inactivation at more positive voltages (>20 mV). The Ca^{2+} current was modelled as a single non-inactivating current.

4. As might be expected, the embryonic neurons possessed a mixture of outward currents that were hard to separate either pharmacologically or through differences in voltage dependence. The delayed rectifier seemed to consist of varying proportions of two currents: a fast-activating K^+ current (with time constants of activation ranging from 0·6 to 2 ms) and a slow K^+ current (with time constants of activation ranging from 5 to 25 ms). The slow current was occasionally seen in isolation.

5. For the Ca^{2+}, fast K^+ and slow K^+ currents the rate of deactivation was faster than would be predicted from the kinetics of activation. This was modelled by allowing the closing rate constant of the channels to be described by one of two different functions of voltage that between them covered the whole range of transmembrane voltage. Although this was done for empirical reasons, it could be interpreted to suggest that the channels have more than one open state and predominantly close from a state that is distinct from the one to which they originally opened.

Although much progress has been made in identifying and characterizing the neural circuits that underlie rhythmic motor patterns in both vertebrates and invertebrates (for reviews see Jacklet, 1989), the reasons why these circuits are able to produce behaviourally appropriate outputs is not self-evident. The operation of a neural circuit depends critically upon the properties of its components: the neurons and their interconnecting synapses. Thus, fundamental understanding of the control of behaviour requires not only the elucidation of the underlying circuits but also a grasp of how, for example, the voltage-gated currents possessed by the neurons determine both their individual properties and the operation of the whole circuit.

The *Xenopus* embryo is an established lower vertebrate model for the control of locomotion (Roberts, Soffe & Dale, 1986; Arshavsky, Orlovsky, Panchin, Roberts & Soffe, 1993). The embryo displays a limited repertoire of behaviours and possesses an extremely simple nervous system and neuroanatomy (Khan & Roberts, 1982*a*, *b*; Roberts & Clarke, 1982). This simplicity has allowed the circuitry underlying the control of swimming to be elucidated (Dale, 1985; Dale & Roberts, 1985; Perrins & Roberts, 1994). During development, the *Xenopus* embryo first becomes capable of swimming at stage 28, the characteristics of the pattern gradually change and become stabilized at stage 32 and they remain fairly constant through to stage 39

* Present address: School of Biological and Medical Sciences, Bute Medical Building, University of St Andrews, St Andrews, Fife KY16 9TS, UK.

(van Mier, Armstrong & Roberts, 1989), after which the motor pattern gradually changes to that typical of the larva at stage 42 (Sillar, Wedderburn & Simmers, 1991) (staging according to Nieuwkoop & Faber, 1956). Although both the swimming motor pattern and the underlying circuitry are simple, it remains unclear why the spinal circuitry is able to produce this particular pattern. This is a non-trivial problem since, under certain circumstances, the same circuitry is clearly capable of generating alternative outputs (Soffe, 1993).

To understand the operation of the swimming circuitry in the *Xenopus* embryo it has been necessary to study the properties of the component neurons in more detail, in particular to characterize their ionic currents. To do this, I have devised a method for isolating the neurons of the central pattern generator for swimming and using whole-cell patch clamp techniques to record their currents (Dale, 1991). Rather than producing mechanistically accurate kinetic models of the ionic currents, my aim has been to characterize the currents sufficiently well to allow Hodgkin–Huxley-style models (Hodgkin & Huxley, 1952) to be generated that accurately reproduce the behaviour of the currents over physiological ranges of voltage and which can then be used in more realistic simulations of the neurons and locomotor circuits.

METHODS

Preparation of neurons

Acutely isolated neurons from the spinal cord of the stage 37/38 *Xenopus* embryo were obtained using methods previously described (Dale, 1991, 1993; Wall & Dale, 1994*a*,*b*). In brief, embryos were anaesthetized in tricaine methanesulphonate (MS222; Sigma), and their spinal cords carefully dissected free. A combination of brief enzymatic treatment (2 min in 10 mg ml^{-1} pancreatin or pronase E (Sigma), in a saline solution comprising (mM): 115 $NaCH_3SO_3$, 2·4 $NaHCO_3$, 3 KCl, 1 $MgCl_2$, 2 $CaCl_2$, 10 Hepes and 10 glucose, pH 7·6) and mechanical dissociation reliably gave a good yield of healthy neurons. These were plated onto poly-D-lysine-coated dishes and left for about 1 h before recordings.

Electrophysiological recordings

Electrodes were fabricated using a Sutter Instruments P87 puller from glass obtained either from World Precision Instruments (TW 150F) or Clark Electromedical Instruments (GC 150F). Conventional whole-cell recording techniques were used. A List EPC7 amplifier together with a DT2831 interface (Data Translation) or an Axopatch 200A and Digidata 1200 interface (Axon Instruments) were used to record and digitize the voltage and current records. Data were acquired to the hard disk of an IBM-compatible PC, while an optical disk was used for long-term storage of experimental records. The recordings had access resistances ranging from 4 to 12 MΩ. Between 70 and 85% of this access resistance was compensated for electronically.

Leak subtraction was performed on all records by either of two methods. For one method, the current of interest was blocked (TTX for the Na^+ current, Cd^{2+} for the Ca^{2+} current) and the remaining leak currents subtracted from the equivalent experimental records from the same cell. In the other method, a scaled negative version of the experimental pulse protocol was given to the same cell. This was subsequently scaled up and added to the experimental records. The scaling factor was usually 2·5. In both cases, the leak currents were obtained immediately before or after each set of experimental records. Both methods gave similar results.

Since my aim was to perform a kinetic analysis of the various currents possessed by the *Xenopus* spinal neurons it was important to allow for the junction potential at the tip of the electrode. Following the methods of Fenwick, Marty & Neher (1982), this was measured as between 6 and 8 mV for the electrolytes used and 8 mV was thus subtracted from the voltage records to correct for this junction potential.

Solutions used

Na^+ and Ca^{2+} currents were recorded by means of a Cs^+ electrolyte (mM): 100 $CsCH_3SO_3$, 1 $CaCl_2$, 6 $MgCl_2$, 20 Hepes, 5 ATP and 10 EGTA, pH 7·4, adjusted to 240 mosmol l^{-1}. The external medium contained (mM): 57·5 NaCl, 57·5 TEA-Cl, 2·4 $NaHCO_3$, 3 KCl, 10 $CaCl_2$, 1 $MgCl_2$, 10 Hepes, 1 4-aminopyridine, pH 7·4, adjusted to 260 mosmol l^{-1}.

K^+ currents were recorded with an electrolyte containing (mM): 100 KCH_3SO_3, 5 $MgCl_2$, 20 Hepes, 5 ATP and 2 BAPTA, pH 7·4, adjusted to 240 mosmol l^{-1} and an external medium containing (mM): 115 NaCl, 2·4 $NaHCO_3$, 3 KCl, 10 $CaCl_2$, 1 $MgCl_2$, 10 Hepes, pH 7·4, adjusted to 260 mosmol l^{-1}.

Adequacy of voltage clamp

To fit valid kinetic models to the voltage clamp records it was important to be convinced of the efficacy of the voltage clamp and space clamp. *Xenopus* spinal neurons both *in vivo* and after dissociation have relatively few short dendrites (< 100 μm). The acutely isolated neurons chosen for this study had at most three short processes little more than a cell body diameter in length (10–15 μm). The adequacy of the voltage clamp was assessed by studying the I–V relations obtained from a series of voltage steps separated by 5 mV. The criterion for effective space clamp was a smoothly activating current, the I–V relation of which could be well fitted in the case of the Na^+ currents by eqn (1) with $g(V,t)$ being given by the steady-state activation of the current, or for the Ca^{2+} and K^+ currents by eqn (3) (see Figs 1*B*, 3*A b*, 6, 7*A b*, 10*A b* and 12*A b*).

Kinetic analysis of ionic currents

Empirical kinetic models of the ionic currents were obtained by following the methods first proposed by Hodgkin & Huxley (1952). In brief, the Na^+ currents were assumed to obey Ohm's law and were described by:

$$I = g(V,t)(V - E), \quad (1)$$

where I is the current, g is the conductance and is a function of transmembrane voltage (V) and time (t), and E is the equilibrium potential for Na^+.

$$g(V,t) = g_{max} m^x h^y \qquad (0 \leqslant m,h \leqslant 1), \quad (2)$$

where g_{max} is a constant and represents the maximum conductance, m an activation variable and h an inactivation variable raised to the powers x and y, respectively.

Both the K^+ and Ca^{2+} currents were modelled using the Goldmann–Hodgkin–Katz equation to describe current flow through the open channel:

$$I_S = g(V,t)P_S\frac{z^2VF^2}{RT}\times\frac{[S]_i - [S]_o e^{-zVF/RT}}{1 - e^{-zVF/RT}}, \quad (3)$$

where P_S is the maximal permeability of the ion S when the current is fully activated, $[S]_o$ and $[S]_i$ the external and internal concentrations of S, respectively, z is the valence of S and the other symbols have their usual thermodynamic meanings. Additionally, the slow and somewhat variable inactivation of these currents was ignored in this first description of the currents. In this case:

$$g(V,t) = m^x \qquad (0 \leqslant m \leqslant 1). \quad (4)$$

The variables m and h are functions of time:

$$\frac{dm}{dt} = \alpha_m(1 - m) - \beta_m \quad (5)$$

and

$$\frac{dh}{dt} = \alpha_h(1 - h) - \beta_h, \quad (6)$$

where α_m is the rate constant of opening and β_m the rate constant of closing, α_h is the rate constant of inactivation and β_h the rate constant of deinactivation.

By solving eqn (5) it can be seen that:

$$m = m_\infty + (m_0 - m_\infty)e^{-t/\tau_m}, \quad (7)$$

where m_0 is the value of m at time $t = 0$,

$$m_\infty = \frac{\alpha_m}{\alpha_m + \beta_m} \quad (8)$$

and

$$\tau_m = \frac{1}{\alpha_m + \beta_m}. \quad (9)$$

Similar solutions can be obtained for eqn (6) to give equivalent expressions for h, h_∞ and τ_h.

The rate constants α_m and β_m can be obtained from eqns (8) and (9):

$$\alpha_m = \frac{m_\infty}{\tau_m} \quad (10)$$

and

$$\beta_m = \frac{1 - m_\infty}{\tau_m}. \quad (11)$$

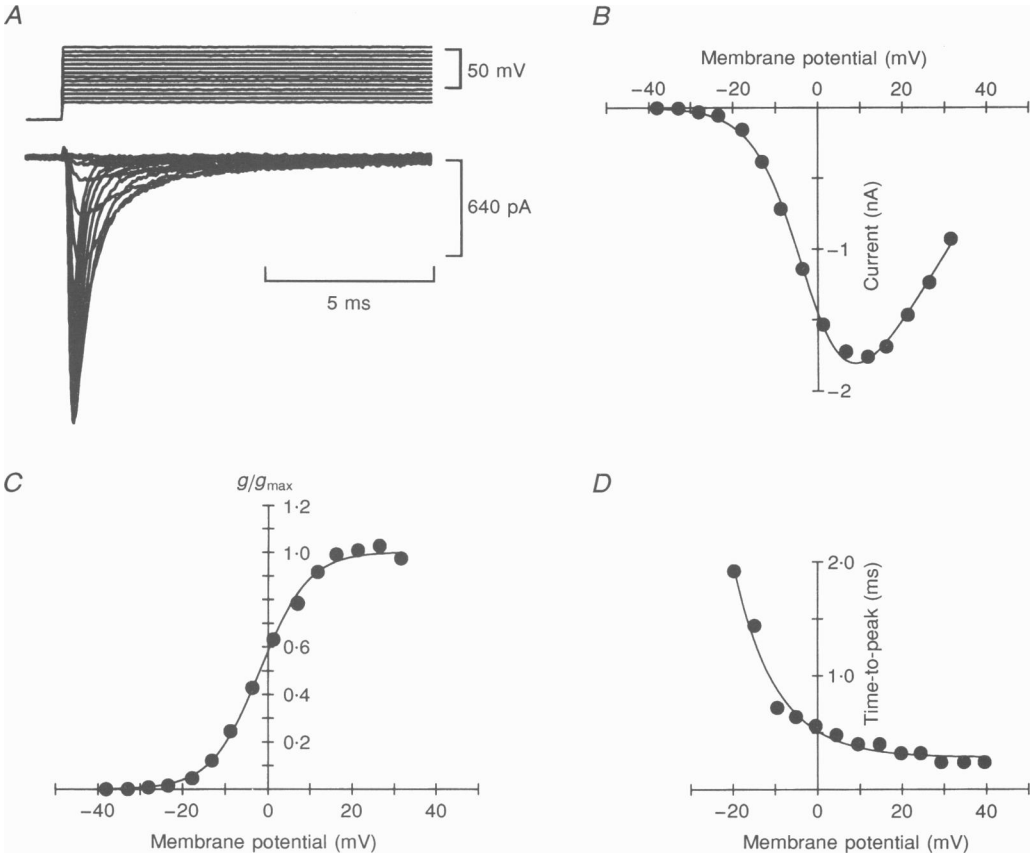

Figure 1. *Xenopus* spinal neurons possess a fast Na^+ current

A, voltage clamp records showing the rapidly activating current. The holding potential was −50 mV. *B*, the *I–V* curve showing the activation of the current. The continuous line is drawn according to eqn (1) (see Methods). *C*, the conductance activation curve for the Na^+ current obtained from the peak current as described in the Methods. The continuous line is the best-fitting Boltzmann equation: $g/g_{max} = (1 + e^{(V + V_{1/2})/k})^{-1}$, where $V_{1/2}$ and k are constants. *D*, the time-to-peak of the current plotted against voltage. The continuous line is the best-fitting exponential, $t = ae^{(V + b)} + c$, where t is the time-to-peak, V the voltage and a, b and c are constants. All data are from a single neuron.

To estimate the rate constants α and β for activation and inactivation, both the steady-state activation and inactivation (to give m_∞ and h_∞) and the time constants of activation and inactivation τ_m and τ_h were measured.

Since it was not possible to voltage clamp the very fast Na^+ relaxation currents, the voltage activation of the Na^+ conductance (g_{Na}) was determined in the following way. First, the Na^+ equilibrium potential (E_{Na}) was estimated by extrapolation of the linear portion of the I–V curve (Fig. 1*B*), where the Na^+ conductance was maximally activated, to the zero current level. The slope of this linear portion of the I–V curve gave an estimate of the maximal Na^+ conductance (Fig. 1*B*) and the conductance at each voltage was estimated using eqn (1) (Fig. 1*C*). Following Hodgkin & Huxley (1952), the conductance activation curve obtained in this way was assumed to represent m_∞^3 (but see Results). The steady-state inactivation variable h_∞ was obtained by conventional means.

The activation of the Ca^{2+} current was obtained by fitting the I–V curve with:

$$I_{Ca}=\frac{1}{1+e^{(V+b)/c}}P_{Ca}\frac{z^2VF^2}{RT}\times\frac{[Ca]_i-[Ca]_o e^{-zVF/RT}}{1-e^{-zVF/RT}}, \quad (12)$$

where the first part of this equation is the Boltzmann equation with b and c being constants and where the second part represents the Goldmann–Hodgkin–Katz equation with the symbols having the same meaning as those in eqn (2). This allowed estimates for both the maximal permeability of the channel to Ca^{2+} (P_{Ca}) and the voltage activation of the Ca^{2+} conductance to be obtained. The activation of the K^+ currents was obtained by studying the activation of the tail currents. The maximal permeability to K^+ was estimated by fitting eqn (3), with $g(V,t)$ being obtained from the activation of the tail currents, to the I–V curves (Figs 10*A b* and 12*A b*).

The time constants for the activation and inactivation of the various currents were obtained by fitting the Hodgkin–Huxley equations to the voltage clamp current records. At voltages negative to those in which significant voltage activation is seen, α and β can still be obtained by studying the kinetics of the relaxation tail currents. However, if the activation kinetics are raised to xth power (x gating particles must be in place for the channel to open) then, since presumably only one gating particle need move to close the channel, the time constant of the tail currents should only be $1/x$ of the duration of the activation time constant. Thus the time constants of the tail currents should be

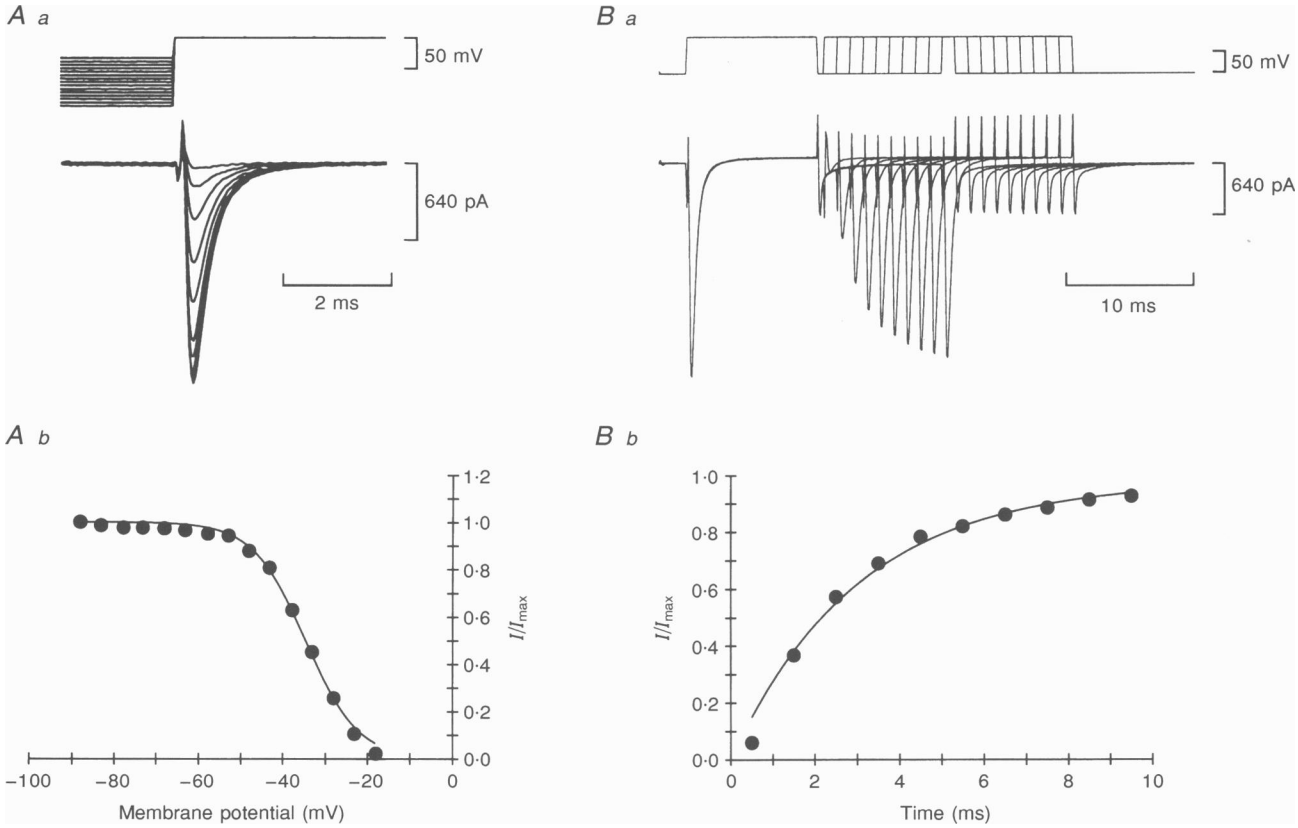

Figure 2. Steady-state inactivation of the Na^+ current

A a, current records evoked by jumps from a holding potential of −50 mV to a fixed test potential of 15 mV from a series of 20 ms prepulses (ranging from −90 to −20 mV). *A b*, the steady-state inactivation curve and best-fitting Boltzmann relation (continuous line) for the Na^+ current. *B a*, paired voltage steps to +20 mV were given from a holding potential of −60 mV. The gap between the pulses was successively widened, allowing more and more of the inactivation to be removed. *B b*, the recovery from inactivation plotted against the time between pulses (data from *B a*). The continuous line is the best-fitting exponential to allow the calculation of τ_h (see text). Data in *A* and *B* are from different neurons.

multiplied by x to represent the activation time constant (Hagiwara & Ohmori, 1982; Huguenard & McCormick, 1992).

To calculate the values of α and β over the whole voltage range it was also necessary to estimate the steady-state value of the gating variable m at voltages at which there was little activation of the current. This was achieved by extrapolating the mean steady-state conductance activation curve (by means of the best-fitting Boltzmann equation, cf. Fig. 1*C*) to more negative potentials. The values of m^x at the desired voltages were then interpolated from this curve and m obtained by taking the appropriate root of the value obtained. This method was used in Fig. 11*C* (8 most negative points) and Fig. 13*C* (9 most negative points).

Curve fitting

Curves were fitted to experimental data using the maximum likelihood method with the simplex algorithm (Press, Flannery, Teukolsky & Vetterling, 1988). These were implemented either in C (Microsoft) or C++ (Symantec).

Computer simulations of ionic currents

The currents were simulated by software written in C++ (Symantec), which ran on an IBM-compatible PC. This implemented the equations given in the text.

RESULTS

The Na^+ current

As might be expected, *Xenopus* embryo neurons possess a fast Na^+ current (Fig. 1). Five cells in which the Na^+ currents were well clamped (see Methods) were analysed by following the classic methods of Hodgkin & Huxley (1952; see Methods). An attempt was made to fit the Hodgkin–Huxley equation to the records of the Na^+ current:

$$I_{Na} = g_{Na}(V - E_{Na})(1 - e^{-t/\tau_m})^3 e^{-t/\tau_h}, \quad (13)$$

where g_{Na} was obtained for each voltage by methods described above, and τ_m and τ_h represent the time constants of activation and inactivation, respectively. This procedure, however, failed to provide a good fit for the observed current records. In the paper by Hodgkin & Huxley (1952), the g_{Na} in eqn (13) represented the Na^+ conductance in the *absence* of any inactivation. The Na^+ currents recorded here inactivated extremely rapidly (Fig. 1*A* and *D*) and it seemed likely that a significant proportion of the Na^+ channels were inactivated at the time of the peak current (from which g_{Na} was estimated). It was therefore necessary

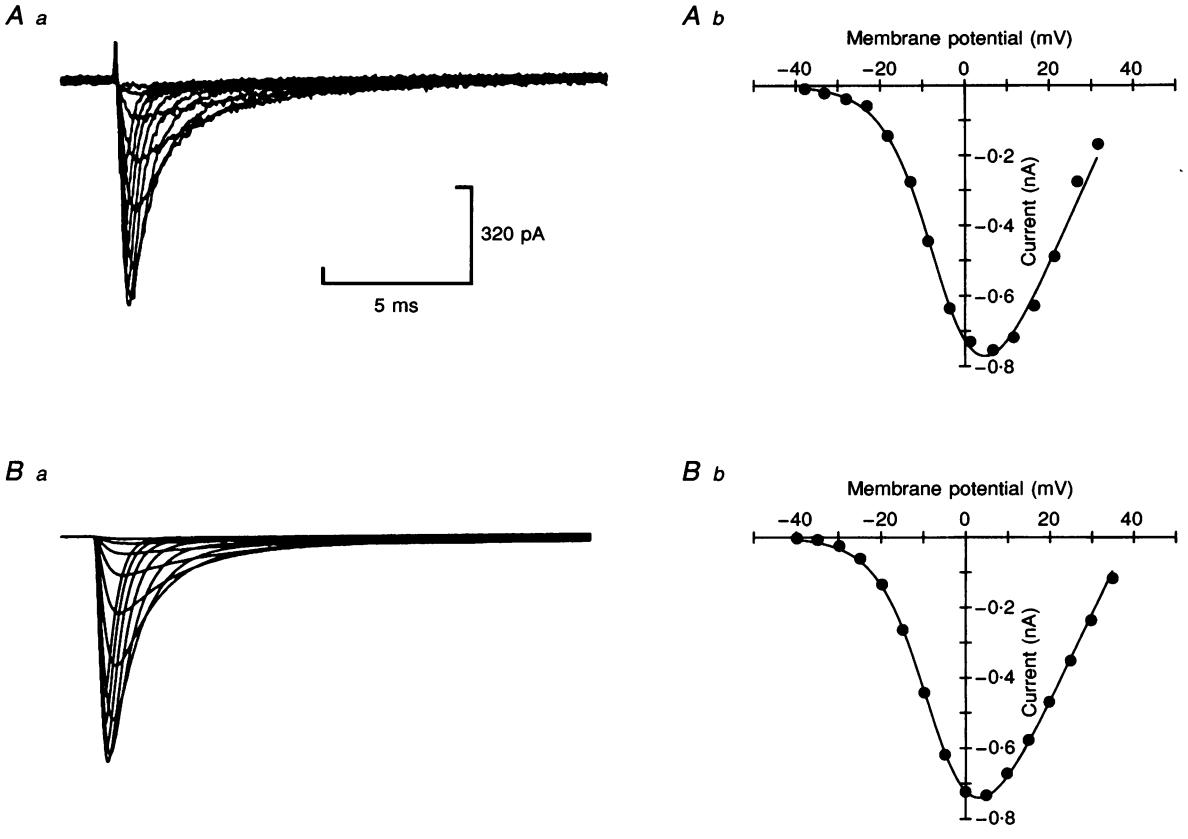

Figure 3. Comparison of the activation of the modelled and experimentally observed Na^+ currents

A a and *A b*, experimentally observed Na^+ currents together with their *I–V* curve. *Ba* and *Bb*, equivalent records for the modelled Na^+ currents and their *I–V* curve. The continuous line on the *I–V* curves corresponds to eqn (1) in the text.

to estimate the degree of channel inactivation (h) at the peak current. This can be done from:

$$h = h_\infty - (h_\infty - h_0)e^{-t/\tau_h}, \quad (14)$$

where h_∞ is the steady-state inactivation and h_0 the inactivation at time $t = 0$. The time-to-peak of the Na^+ current at each voltage was thus measured and expressed as a simple exponential function of voltage (Fig. 1*D*), which could then be used to calculate the time-to-peak for use in eqn (14). The time constant of inactivation (τ_h) was then estimated by fitting an exponential to the falling phase of the current record. This therefore enabled the degree of inactivation to be calculated. The Na^+ conductance activated at each voltage (in the absence of inactivation) could then be determined by:

$$g'_{Na} = g_{Na}/h. \quad (15)$$

When the corrected conductance (g'_{Na}) was used in eqn (13), an excellent correspondence between the amplitude of the observed and predicted current records could be achieved.

While the parameter m_∞ was estimated as the cube root of the corrected conductance (g'_{Na}) activation curve, h_∞ the inactivation parameter was estimated from the steady-state inactivation curves (Fig. 2*A a*). For levels of membrane potential where there was little channel activation, the τ_h was measured by using a standard paired-pulse protocol to study the removal of inactivation (Fig. 2*B a*). The recovery from inactivation at each voltage was then plotted against time (Fig. 2*B b*) and fitted with:

$$I/I_{max} = 1 - e^{-t/\tau_h}, \quad (16)$$

to give an estimate of τ_h. For all of these parameters, the results from the five cells were averaged to give a mean value at each voltage. The forward and backward rate constants of activation were estimated from eqns (10) and (11) and the following functions were fitted to plots of α_m and β_m against voltage:

$$\alpha_m = \frac{8{\cdot}67}{1 + e^{(V-1{\cdot}01)/12{\cdot}56}} \quad (17)$$

and

$$\beta_m = \frac{3{\cdot}82}{1 + e^{-(V+9{\cdot}01)/9{\cdot}69}}. \quad (18)$$

Similarly, the rate constants for inactivation α_h and β_h were plotted against voltage and fitted with the following equations:

$$\alpha_h = 0{\cdot}08e^{-(V+38{\cdot}88)/26} \quad (19)$$

and

$$\beta_h = \frac{4{\cdot}08}{1 + e^{-(V-5{\cdot}09)/10{\cdot}21}}. \quad (20)$$

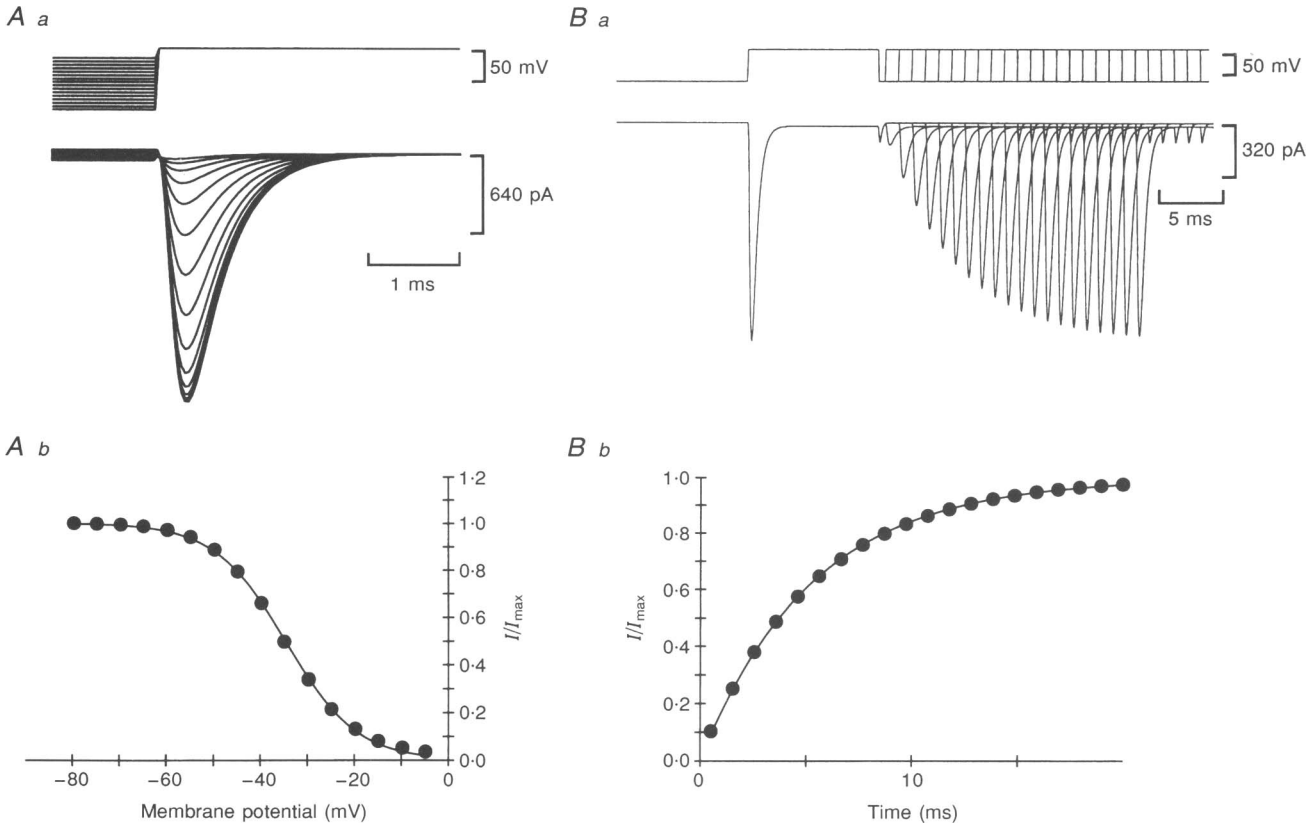

Figure 4. The steady-state inactivation of the modelled Na^+ current
The parts of this figure are exactly equivalent to those of Fig. 2.

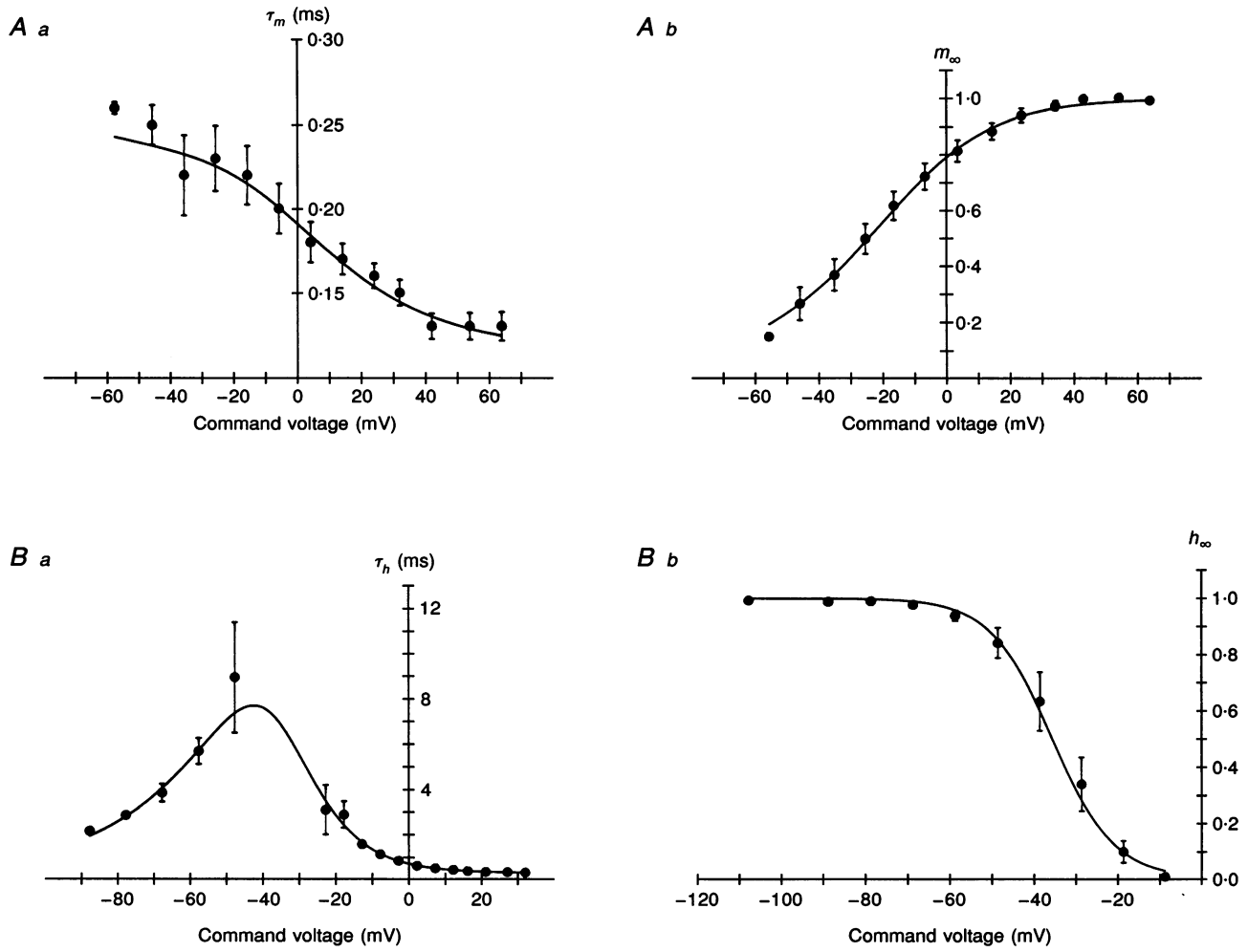

Figure 5. Plots of the experimentally determined time constants of activation (*A a*) and inactivation (*B a*) and the m_∞ and h_∞ curves for the Na^+ current (*A b* and *B b*, respectively)

The continuous lines in *A a* and *B a* are from eqn (9), while those in *A b* and *B b* are from eqn (8) (see Methods). In *B a* the most negative 5 points are determined from the time constants for removal of inactivation (see text and Fig. 2*B a*). Bars represent 1 S.E.M.

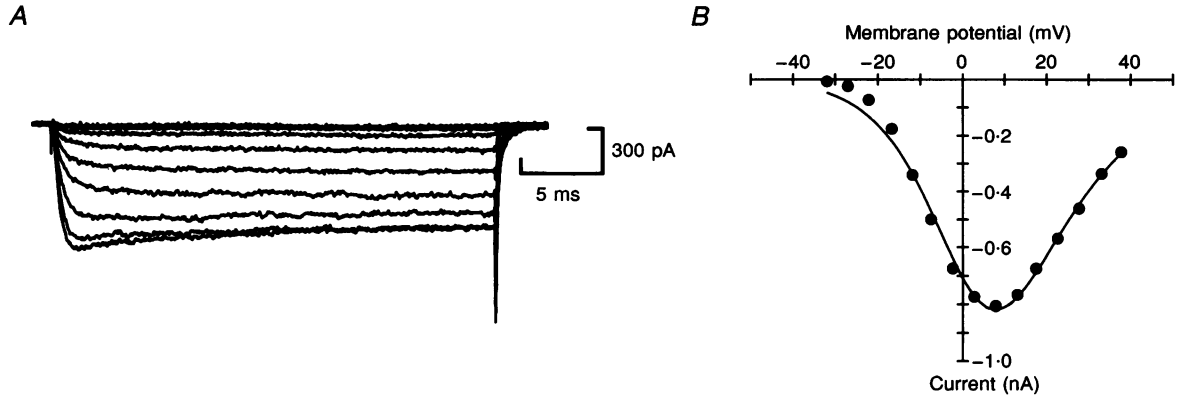

Figure 6. *Xenopus* embryo spinal neurons possess a Ca^{2+} current that shows slow inactivation at positive potentials

A, superimposed current records obtained from voltage steps from a holding potential of −50 mV. *B*, the *I–V* curve for the Ca^{2+} current of the same neuron. Continuous line is drawn according to eqn (12) in the text.

When the Na^+ current was modelled using these rate constants, a very good correspondence between the simulated currents and those recorded in real neurons was observed (Figs 3 and 4). Furthermore, a very good fit between the predicted values of τ_m, τ_h, m_∞ and h_∞ and the experimentally determined values was obtained (Fig. 5).

Ca^{2+} currents

Xenopus spinal neurons possess a Ca^{2+} current that is probably composed of at least two kinetically somewhat similar underlying components: ω-conotoxin GVIA-sensitive and -insensitive currents (Wall & Dale, 1994*a*). These Ca^{2+} currents show some slow inactivation at more positive potentials (>20 mV, Fig. 6). The underlying components were not separable on the basis of voltage protocols alone. Therefore, for simplicity, the total Ca^{2+} current was modelled as a single current. Since inactivation only became evident above +20 mV, a voltage range that neurons experience only briefly, if at all, during physiological activity, this slow and somewhat variable inactivation shown by the total Ca^{2+} current was ignored. By trial and error, it was determined that the best fits of the Hodgkin–Huxley equations could be obtained if the activation variable was raised to the second power. Thus, for the Ca^{2+} current, eqn (4) became:

$$g_{Ca} = m^2 \tag{21}$$

and the equation:

$$I_{Ca} = \frac{1}{1+e^{(V+b)/c}} P_{Ca} \frac{z^2VF^2}{RT} \times \frac{[Ca]_i - [Ca]_o e^{-zVF/RT}}{1-e^{-zVF/RT}} (1-e^{-t/\tau_m})^2 \tag{22}$$

was fitted to the current records, where b, c and P_{Ca} are constants, and were obtained from the data as described in the Methods and τ_m, the time constant of activation, was the free variable that was adjusted to achieve the best fit. The parameter m_∞ was estimated as the square root of conductance (g_{Ca}) activation curve (Figs 6*B* and 7*A b*). For both these parameters, the results from the nine cells were averaged to give a mean value at each voltage. The rate of deactivation at potentials negative to −35 mV was measured in five cells by studying the tail currents to obtain estimates for α and β at these lower potentials. The forward and backward rate constants of activation were estimated from eqns (10) and (11). It soon became apparent that the plot of β against voltage could not be fitted by a

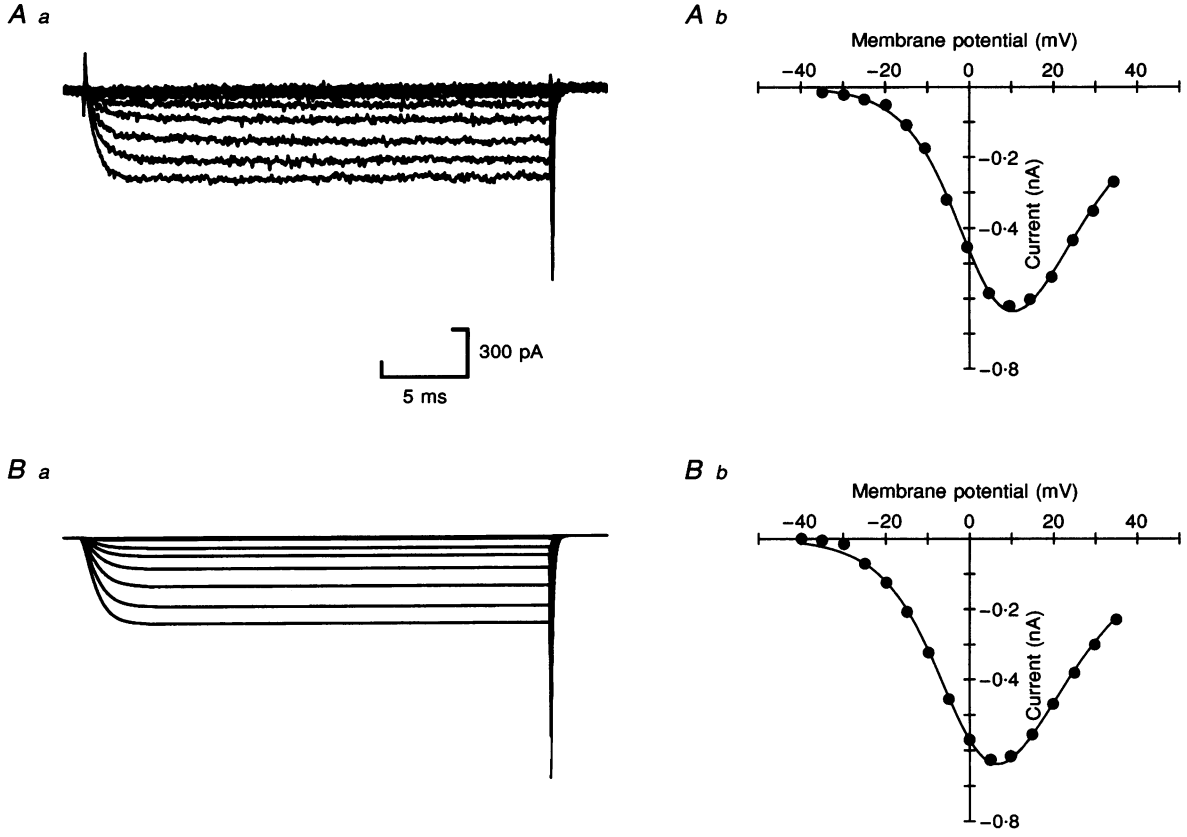

Figure 7. Comparison of the activation of the modelled and experimentally observed Ca^{2+} currents

A a and *A b*, experimentally observed Ca^{2+} currents from a single neuron together with their *I–V* curve. *Ba* and *B b*, equivalent records for the modelled Ca^{2+} currents and their *I–V* curve. The continuous line on the *I–V* curves corresponds to eqn (12) in the text.

single function over its whole range (Fig. 8A). In consequence, this closing rate constant was given dual kinetics to allow the data to be modelled accurately (cf. Huguenard & McCormick, 1992). The following functions were thus fitted to plots of α and β against voltage:

$$\alpha = \frac{4{\cdot}05}{1+e^{-(V-15{\cdot}32)/13{\cdot}57}}, \quad (23)$$

$$\beta_1 = \frac{1{\cdot}28}{1+e^{(V+5{\cdot}39)/12{\cdot}11}} \quad (V > -25 \text{ mV}) \quad (24)$$

and

$$\beta_2 = \frac{0{\cdot}093(V+10{\cdot}63)}{e^{V+10{\cdot}63}-1} \quad (V \leqslant -25 \text{ mV}). \quad (25)$$

Using these rate constants, a good correspondence between the modelled and observed Ca^{2+} currents was obtained (Fig. 7). In addition, the predicted values of τ_m and m_∞ matched very well with those determined from experiments (Fig. 8) over the whole voltage range. Although the current was modelled with dual kinetics for empirical reasons, the change in the kinetics necessary for deactivation may have a physical basis and perhaps suggest that the channels have multiple open states and predominantly close from an open state that is distinct from the one to which they originally opened (see Discussion).

K^+ currents

As might be expected, *Xenopus* neurons possess a complex mixture of K^+ currents that are not readily separable, including a Na^+-dependent K^+ current, voltage-dependent K^+ currents and a slowly activating Ca^{2+}-dependent K^+ current (Wall & Dale, 1995). The Na^+-dependent K^+ current has been modelled in a previous paper (Dale, 1993). No attempt is made in this paper to model the Ca^{2+}-dependent K^+ current. The purely voltage-dependent K^+ currents

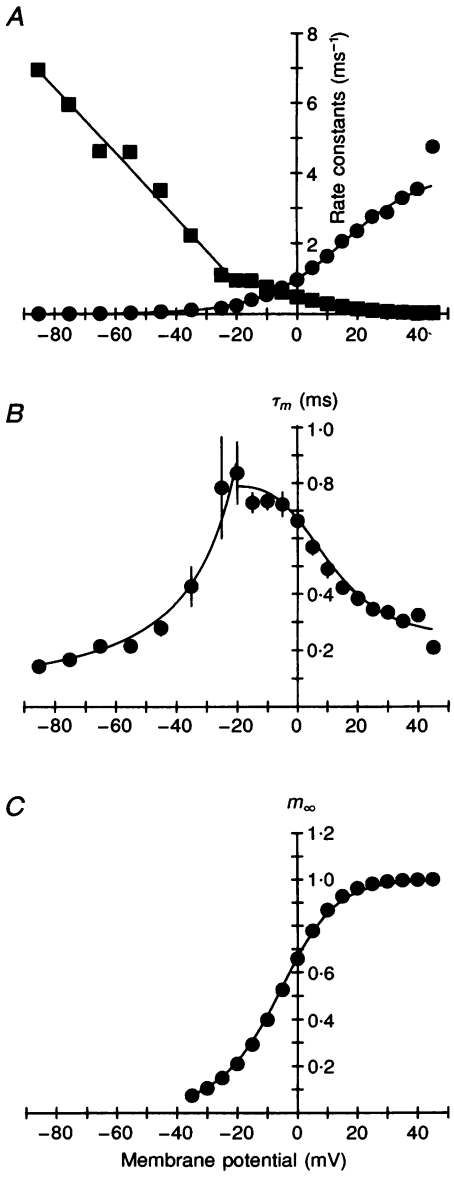

Figure 8. Kinetic parameters for the Ca^{2+} current

A, plots of α (●) and β (■) *versus* voltage obtained from eqns (10) and (11), respectively. While α can be fitted by a single function of voltage, 2 functions are required to fit β. *B*, the measured time constants together with the values predicted from the model of the current. The 6 most negative points were obtained from the kinetics of deactivation. *C*, a plot of m_∞ *versus* voltage showing the close agreement between the experimentally determined points and the curve predicted by the model. Bars represent 1 S.E.M. and are too small to be seen in *C*.

consist of an A-current, which is small and present in only a minority of neurons, and two other voltage-dependent currents (Figs 9, 10 and 12). Since the A-current was a rare and minor component of the outward currents, and undergoes strong inactivation at physiological voltages, it was left out of this first description of the currents. The other two K^+ currents could be said to constitute the delayed rectifier and were very difficult to separate. Very occasionally, one of the components, a slowly activating current, was fortuitously seen in isolation (4 cells, Fig. 12). In the vast majority of neurons studied, careful inspection of the kinetics of activation and the tail currents showed that the current consisted of a mixture of the slow current and a much faster activating current (Fig. 9*A* and *B*). It was not possible to separate these currents either pharmacologically or through the use of voltage protocols. However, their kinetics of activation and deactivation were quite distinct. I was thus able to fit unambiguously the total K^+ currents with a sum of two currents described by the Hodgkin–Huxley equations:

$$I_T = (1-f)I_{K1} + fI_{K2}, \quad (26)$$

where I_T represents the total current, I_{K1} and I_{K2} are the two components of the K^+ current and f is the fraction of the total current carried by I_{K2}. This allowed the kinetic parameters of activation and conductance for the two currents to be measured from the data by this fitting procedure (Fig. 9*A*). To allow the kinetics of relaxation for the two currents to be analysed separately, the tail currents were fitted by a sum of two exponentials (Fig. 9*B*). Since the time constants for activation and deactivation obtained by measuring the slow current both in isolation and in combination with the fast current were very similar, the data obtained by the two methods were pooled. Once again it proved necessary to model both the fast and slow K^+ currents with dual kinetics: the relaxation currents decayed faster than would be predicted from the activation kinetics. The closing rate constant β was thus fitted by two separate functions depending on the voltage range (Figs 11*A* and 13*A*).

For the fast K^+ current it was found that the activation kinetics were best described by assuming $x = 4$ in eqn (4). Although the activation kinetics were raised to the 4th power, the kinetics of deactivation were found empirically to be better described as if they were raised to the 2nd power (and thus assuming that 2 out of 4 gating particles had to change state for channel closure). To allow for this, the time constants of the tail currents were doubled rather

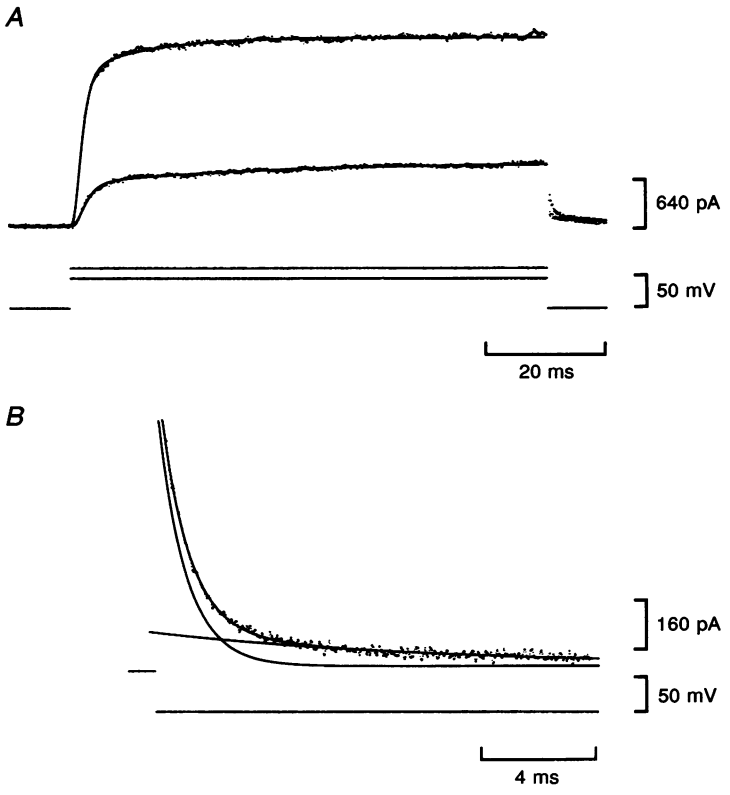

Figure 9. The delayed rectifier consists of two K^+ currents with distinct kinetics

A, fits of the Hodgkin–Huxley equations (continuous lines) to records of the K^+ currents, showing that the currents consist of the sum of a fast and slow K^+ current. *B*, the tail currents (from a different neuron) also have 2 kinetic components which correspond to the 2 distinct components of activation. The continuous line superimposed upon the current record is the sum of the 2 exponentials shown separately on the figure.

than quadrupled (see Methods). The following equations were fitted to plots of the rate constants α and β against voltage (Fig. 11*A*):

$$\alpha = \frac{3{\cdot}1}{1+e^{-(V-29{\cdot}5)/23{\cdot}3}}, \tag{27}$$

$$\beta_1 = \frac{0{\cdot}44}{1+e^{(V+6{\cdot}98)/16{\cdot}19}} \qquad (V > -45 \text{ mV}) \tag{28}$$

and

$$\beta_2 = 0{\cdot}1e^{-(V+11{\cdot}67)/24{\cdot}96} \qquad (V \leqslant -45 \text{ mV}). \tag{29}$$

This allowed an accurate model of the fast K^+ current to be constructed, which showed very similar activation and relaxation kinetics to the observed fast current in these neurons (Figs 10 and 11).

For the slow currents the activation kinetics were adequately fitted by assuming $x = 1$ in eqn (4). When the rate constants α and β for the slow K^+ current were plotted against voltage (Fig. 13*A*) the following functions were found to describe the data:

$$\alpha = \frac{0{\cdot}16}{1+e^{-(V-4{\cdot}69)/7{\cdot}74}}, \tag{30}$$

$$\beta_1 = \frac{0{\cdot}04}{1+e^{(V-16{\cdot}07)/6{\cdot}1}} \qquad (V > -30 \text{ mV}) \tag{31}$$

and

$$\beta_2 = \frac{0{\cdot}0012(V-3{\cdot}63)}{e^{(V-3{\cdot}63)/2{\cdot}41}-1} \qquad (V \leqslant -30 \text{ mV}). \tag{32}$$

Once again, these rate constants allowed an accurate model of the slow K^+ current to be constructed (Figs 12 and 13).

DISCUSSION

Voltage-gated currents present in acutely isolated *Xenopus* neurons

Rather than to produce mechanistically accurate models of ion channel gating, the aim of this paper was to generate accurate empirical Hodgkin–Huxley-style models of the principal currents possessed by *Xenopus* neurons, which

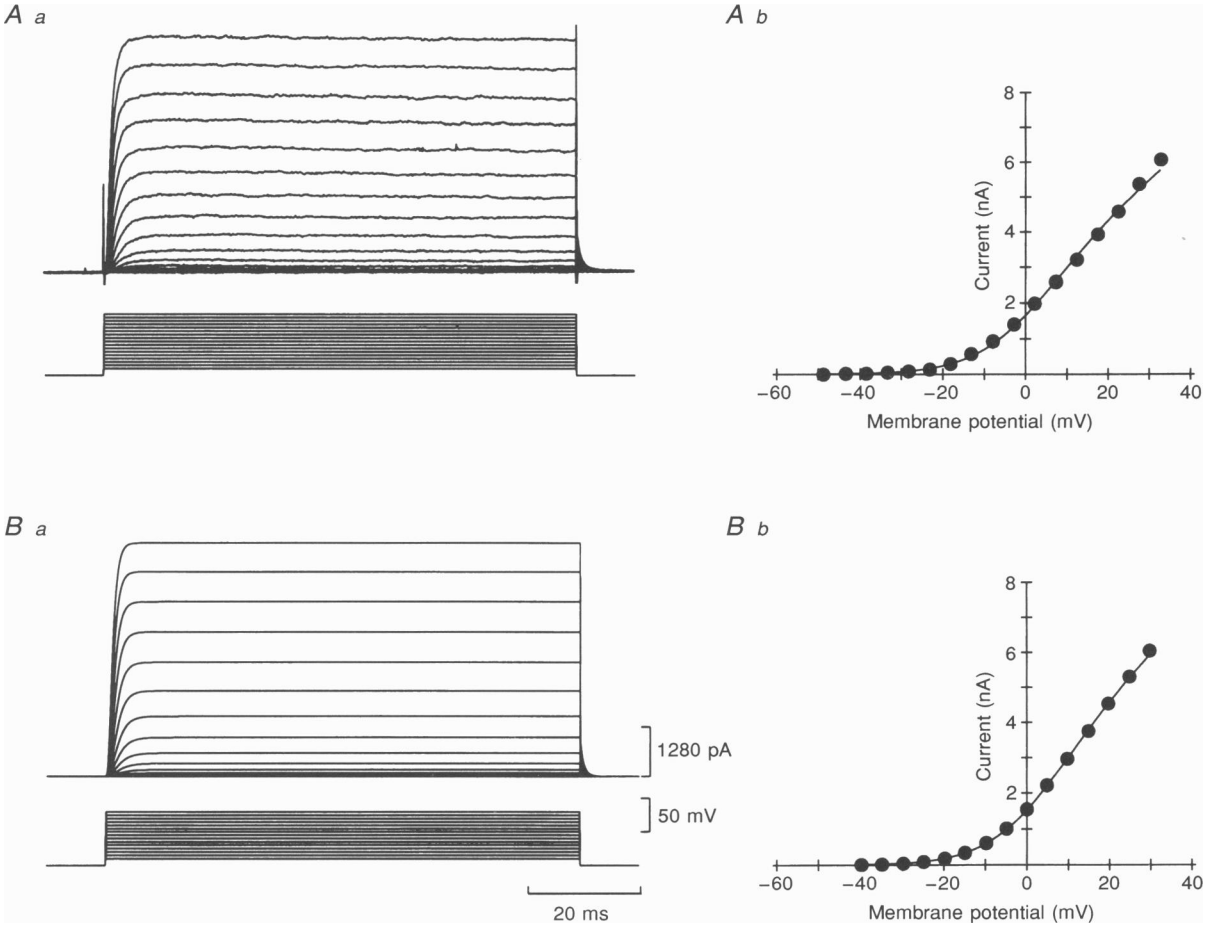

Figure 10. Comparison of the experimentally observed fast K^+ current with its model

A a, voltage clamp records of K^+ currents which had very little of the slow component together with its *I–V* curve (*A b*). *Ba*, equivalent records for the modelled fast K^+ current. *Bb*, the *I–V* curve for the modelled fast K^+ current. Continuous lines in *A a* and *B b* are drawn according to eqn (3) in the text.

could then be used in simulations of the spinal network. *Xenopus* embryo neurons appear to possess a relatively limited set of channels: a fast Na^+ channel, a mixture of kinetically similar Ca^{2+} channels, a set of voltage-gated K^+ channels with distinct kinetics, a Na^+-dependent K^+ current (Dale, 1993) and a slowly activating Ca^{2+}-dependent K^+ current (Wall & Dale, 1995). The great majority of neurons studied, including multipolar, unipolar and commissural-like cells, possessed these currents in varying proportions. These morphologies encompass the excitatory and inhibitory interneurons as well as motoneurons (Dale, 1991). Although no detailed statistical studies have been performed, no obvious correlations between densities of currents and morphological types have so far been evident.

While the Na^+-dependent and Ca^{2+}-dependent K^+ currents are described elsewhere (Dale, 1993; Wall & Dale, 1995), the voltage-gated currents have been modelled in this paper as a single Na^+ current, a single Ca^{2+} current and two K^+ currents. Although the Na^+ current is likely to be a single current, the Ca^{2+} and K^+ currents are probably mixtures of several distinct channels. The Ca^{2+} current can be separated into components pharmacologically by the use of ω-conotoxin GVIA (Wall & Dale, 1994*a*). However, the subcomponents appear very similar kinetically and thus, as a first approximation, the Ca^{2+} currents can be modelled by a single channel. Although the K^+ currents are not readily separable, either by voltage protocols or pharmacologically, it was necessary to model the delayed rectifier as a sum of two currents: fast-activating and slowly activating components. This is likely to be a valid approach since the slow component of the K^+ currents has very occasionally been seen in isolation and the delayed rectifier appears to be made up of varying proportions of these two component currents. It is still possible that further components of the delayed rectifier remain undescribed, but the combination of the fast and slow currents gives a good first approximation of the observed voltage-gated K^+ currents.

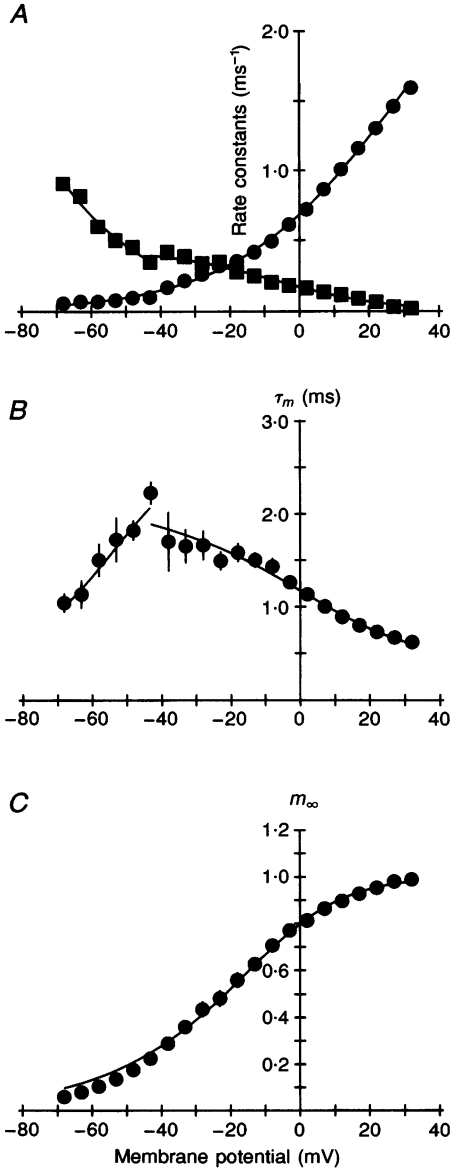

Figure 11. Kinetic parameters for the fast K^+ current

A, plots of α (●) and β (■) *versus* voltage obtained from eqns (10) and (11), respectively. While α can be fitted by a single function of voltage, 2 functions are required to fit β. *B*, the measured time constants together with the values predicted from the model of the current. The 5 most negative points were obtained from the kinetics of deactivation. *C*, a plot of m_∞ *versus* voltage showing the close agreement between the experimentally determined points and the curve predicted by the model. Bars represent 1 S.E.M.

Comparison with the currents present in cultured *Xenopus* neurons

Ionic currents have been studied in cultured *Xenopus* and *Ambystoma* spinal neurons that have differentiated from their dissociated neural plate precursors *in vitro* (Barish, 1986; O'Dowd, Ribera & Spitzer, 1988; Harris, Henderson & Spitzer, 1988). Although no detailed kinetic analysis has been made of the currents in the cultured neurons, they do appear broadly similar to the currents of the acutely isolated neurons reported here. For example, careful inspection of the records for the voltage-gated K^+ currents in the cultured neurons (e.g. Figs 9 and 11 of O'Dowd *et al.* 1988; Fig. 1 of Ribera & Spitzer, 1987) suggests the existence of both fast and slow components. Indeed, the 'young' neurons in these studies appeared to have voltage-gated currents with slower kinetics of activation than those in the 'older' neurons (O'Dowd *et al.* 1988). These slower currents might correspond to the slow K^+ current described here, but the reported time to half-maximal amplitude (3–6 ms over the range −5 to 25 mV) may be somewhat shorter than might be expected from the corresponding time constants reported for the slow current in this paper (6–12 ms, which is the time to approximately 63% of maximal value). In addition, the time to half-maximal amplitude of the faster K^+ current in the older neurons (2–4 ms, O'Dowd *et al.* 1988) is rather longer than might be expected from the corresponding time constants of activation reported for the fast K^+ current in this paper (0·7–1·3 ms). Neither do the kinetics of the fast and slow K^+ currents that I have described here readily match up with the single channel properties of K^+ channels described in *Xenopus* neurons (Harris *et al.* 1988). The acutely isolated neurons in this study were taken from stage 37/38 embryos and therefore correspond to the 'older' neurons in the above studies. It is therefore tempting to equate the currents in the two studies. However, given the discrepancies between the kinetics of the two sets of currents, caution needs to be exercised in making direct comparisons between the currents reported in this paper and those of the cultured neurons. Transient K^+ and Ca^{2+} currents have also been described in the cultured *Xenopus* neurons (Ribera & Spitzer, 1990; Gu & Spitzer, 1993). While A-currents have been observed in a proportion of acutely isolated neurons, T-type Ca^{2+} currents have not been seen so far. This may be due either to a genuine difference between the acutely isolated neurons and those in culture, which may express different complements of channels *in vitro*, or to localization of the T-type channels on distal processes which may be lost during the acute dissociation.

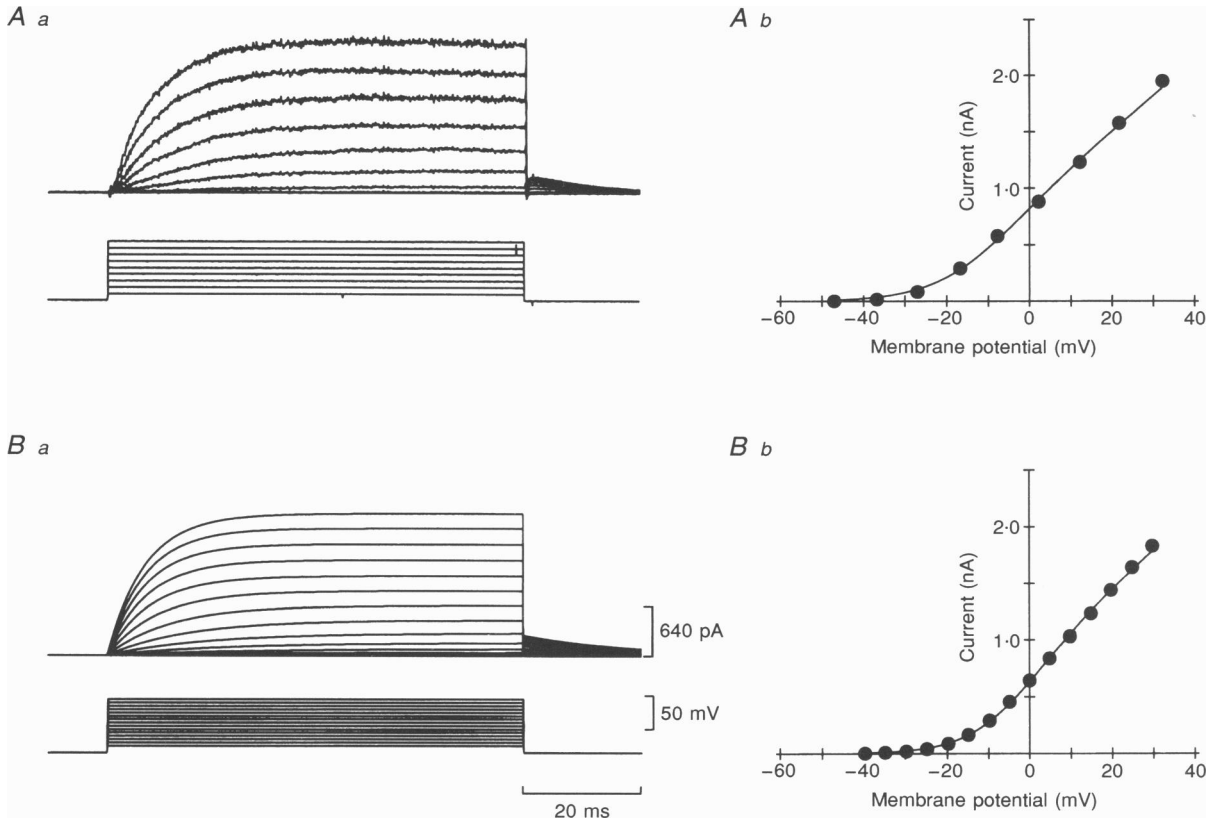

Figure 12. Comparison of the experimentally observed slow K^+ current with its model

A a, voltage clamp records of the slow K^+ currents together with the *I–V* curve from the same neuron (*A b*). *Ba*, equivalent records for the modelled slow K^+ current. *Bb*, the *I–V* curve for the modelled slow K^+ current. Continuous lines in *A b* and *Bb* are drawn according to eqn (3) in the text.

Comparison of K^+ currents with those found elsewhere

Slowly activating K^+ currents have been described in a variety of other neurons. For example, in the frog node of Ranvier, a very slowly activating K^+ current has been observed (Dubois, 1981). However, the time constants of activation for this current are considerably longer than those reported for the slowly activating current described here. More similar currents have been reported in the hippocampal, lateral geniculate and cortical pyramidal neurons (Storm, 1988, 1990; Spain, Schwindt & Crill, 1991; Budde, Mager & Pape, 1992). The pharmacology of these slow currents is somewhat variable, although some are blocked by TEA and are insensitive to 4-aminopyridine (Storm, 1990; Budde *et al.* 1992).

The fast-activating K^+ current is probably more akin to I_D, a K^+ current which undergoes slow inactivation (Storm, 1988). Although the inactivation properties of the fast current have not been studied in detail, this current does appear to inactivate, with a slow time constant of a few hundred milliseconds, in a manner similar to I_D (N. Dale, personal observations). I_D can often be blocked by low levels of 4-aminopyridine and is relatively insensitive to TEA (Storm, 1988). However, the fast current described here can be partially blocked by 50–500 μM TEA. Indeed, although these levels of TEA also block the slow current, they may block proportionally more of the fast current (N. Dale, personal observations).

Possible roles for currents

Although the Ca^{2+} currents are small in these neurons relative to the size of the Na^+ current, they are subject only to very slow voltage-dependent inactivation. The Ca^{2+} currents could therefore be important for spike initiation and the repetitive firing in these neurons (Wall & Dale,

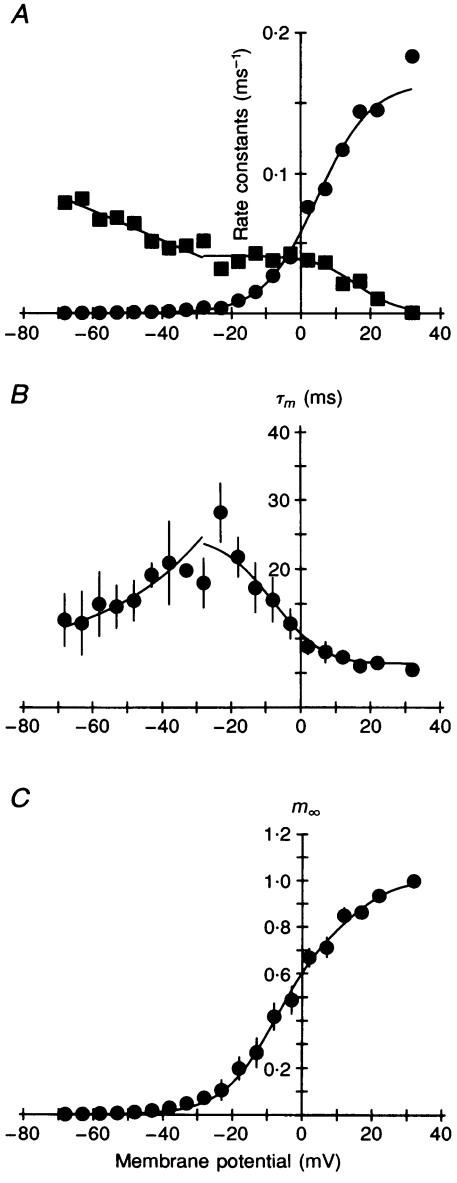

Figure 13. Kinetic parameters for the slow K^+ current

A, plots of α (●) and β (■) *versus* voltage obtained from eqns (10) and (11), respectively. While α can be fitted by a single function of voltage, 2 functions are required to fit β. *B*, the measured time constants together with the values predicted from the model of the current. The 8 most negative points were obtained from the kinetics of deactivation. *C*, a plot of m_∞ *versus* voltage showing the close agreement between the experimentally determined points and the curve predicted by the model. Bars represent 1 S.E.M.

1994*a*; Dale, 1995). The two K^+ currents constitute the delayed rectifier for these neurons and, as such, could contribute to repolarization of the action potential. The slow K^+ current may activate rather too slowly by itself to perform a rapid enough repolarization of the membrane potential during the action potential (Dale, 1995). However, since the slow current has long relaxation currents it may well be important in regulating the frequency of firing in these neurons and space out successive action potentials (Dale, 1995). This slow current may also play an important role in the generation of the swimming motor pattern, in which a slowly activating K^+ current has been proposed to limit firing during the mid-cycle region of the swimming cycle (Wall & Dale, 1994*b*).

Switched kinetics

The Ca^{2+} current and the two K^+ currents could only be modelled accurately by allowing the deactivation of the current to have kinetics distinct from the activation and this was achieved by fitting the closing rate constant β with two functions dependent on voltage over distinct voltage ranges. This was done purely for empirical reasons to ensure that the modelled currents had accurate relaxation kinetics. However, such an empirical model may have some physical basis. For example, the channels could have two open states, opening predominantly to state 1 and closing predominantly from state 2:

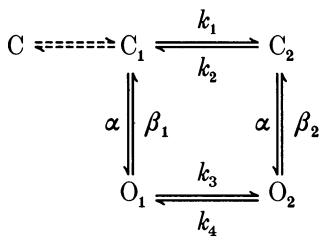

where C represents the closed state and O the open state of the channel, and k_1, k_2, k_3 and k_4 are rate constants.

While the kinetics of this scheme are potentially very complex, if $\alpha \gg k_1$ and $\beta_2 \gg k_4$, then the opening kinetics would be largely determined by α and β_1 while the closing kinetics would be determined largely by α and β_2. If this explanation is correct then there should be a minor component of the relaxation current with a longer time constant that is determined by α and β_1. I have not managed to resolve such a component in these experiments, suggesting that it is either too small or not sufficiently different to detect with dual-exponential fitting procedures.

Improvements to the models

While the purist might demand mechanistically more realistic models, my aim has been to produce accurate and simple renditions of the behaviour of the currents suitable for incorporation into computer simulations of spinal circuitry. On this basis, the most serious short-coming is the fact that the slow inactivation of the K^+ and Ca^{2+} currents has not been modelled. The inactivation of these currents has time constants of several hundreds of milliseconds, and therefore is probably not an important factor for the operation of the spinal network over short time intervals (a few seconds). However, the motor pattern for swimming in the *Xenopus* embryo does undergo slow time-dependent changes, which may depend, at least in part, on the slow inactivation of the voltage-gated ion channels. Thus, a full understanding of the dynamics of a swimming episode, the way the frequency of motor discharge changes with time and the mechanisms of self-termination awaits description of the slow inactivation of both the inward and outward currents of the spinal neurons.

ARSHAVSKY, Y. I., ORLOVSKY, G. N., PANCHIN, Y. V., ROBERTS, A. & SOFFE, S. R. (1993). Neuronal control of swimming locomotion: analysis of the pteropod mollusc *Clione* and embryos of the amphibian *Xenopus*. *Trends in Neurosciences* **16**, 227–233.

BARISH, M. E. (1986). Differentiation of voltage-gated potassium current and modulation of excitability in cultured amphibian spinal neurons. *Journal of Physiology* **375**, 229–250.

BUDDE, T., MAGER, R. & PAPE, H.-C. (1992). Different types of potassium outward current in relay neurons acutely isolated from the rat lateral geniculate nucleus. *European Journal of Neuroscience* **4**, 708–722.

DALE, N. (1985). Reciprocal inhibitory interneurons in the *Xenopus* embryo spinal cord. *Journal of Physiology* **363**, 61–70.

DALE, N. (1991). The isolation and identification of spinal neurons that control movement in the *Xenopus* embryo. *European Journal of Neuroscience* **3**, 1025–1035.

DALE, N. (1993). A large, sustained Na^+- and voltage-dependent K^+ current in spinal neurons of the frog embryo. *Journal of Physiology* **462**, 349–372.

DALE, N. (1995). Experimentally derived model for the locomotor pattern generator in the *Xenopus* embryo. *Journal of Physiology* **489**, 489–510.

DALE, N. & ROBERTS, A. (1985). Dual-component amino-acid-mediated synaptic potentials: excitatory drive for swimming in *Xenopus* embryos. *Journal of Physiology* **363**, 35–59.

DUBOIS, J. M. (1981). Evidence for the existence of three types of potassium channels in the Ranvier node membrane. *Journal of Physiology* **318**, 297–316.

FENWICK, E. M., MARTY, A. & NEHER, E. (1982). A patch-clamp study of bovine chromaffin cells and of their sensitivity to acetyl choline. *Journal of Physiology* **331**, 577–597.

GU, X. & SPITZER, N. C. (1993). Low-threshold Ca^{2+} current and its role in spontaneous elevations of intracellular Ca^{2+} in developing *Xenopus* neurons. *Journal of Neuroscience* **13**, 4936–4948.

HAGIWARA, S. & OHMORI, H. (1982). Studies of Ca^{2+} channels in rat clonal pituitary cells with patch electrode voltage clamp. *Journal of Physiology* **331**, 231–252.

HARRIS, G. L., HENDERSON, L. P. & SPITZER, N. C. (1988). Changes in densities and kinetics of delayed rectifier potassium channels during neuronal differentiation. *Neuron* **1**, 739–750.

HODGKIN, A. L. & HUXLEY, A. F. (1952). A quantitative description of membrane current and its application to conduction and excitation in nerve. *Journal of Physiology* **117**, 500–544.

HUGUENARD, J. R. & MCCORMICK, D. A. (1992). Simulation of the currents involved in rhythmic oscillations in thalamic relay neurons. *Journal of Neurophysiology* **68**, 1373–1383.

JACKLET, J. W. (1989). *Neuronal and Cellular Oscillators.* Dekker, New York.

KAHN, J. A. & ROBERTS, A. (1982*a*). The central nervous origin of the swimming motor pattern in embryos of *Xenopus laevis*. *Journal of Experimental Biology* **99**, 185–196.

KHAN, J. A. & ROBERTS, A. (1982*b*). Experiments on the central pattern generator for swimming in amphibian embryos. *Philosophical Transactions of the Royal Society* B **296**, 229–243.

NIEUWKOOP, P. D. & FABER, J. (1956). *Normal Tables of Xenopus laevis (Daudin).* North Holland, Amsterdam.

O'DOWD, D. K., RIBERA, A. B. & SPITZER, N. C. (1988). Development of voltage-dependent calcium, sodium and potassium currents in *Xenopus* spinal neurons. *Journal of Neuroscience* **8**, 792–805.

PERRINS, R. J. & ROBERTS, A. (1994). Cholinergic contribution to excitation in a spinal locomotor central pattern generator in *Xenopus* embryos. *Journal of Neurophysiology* **73**, 1013–1019.

PRESS, W. H., FLANNERY, B. P., TEUKOLSKY, S. A. & VETTERLING, W. T. (1988). *Numerical Recipes in C. The Art of Scientific Computing.* Cambridge University Press, Cambridge, UK.

RIBERA, A. B. & SPITZER, N. C. (1987). Both barium and calcium activate neuronal potassium currents. *Proceedings of the National Academy of Sciences of the USA* **84**, 6577–6581.

RIBERA, A. B. & SPITZER, N. C. (1990). Differentiation of I_{KA} in amphibian spinal neurons. *Journal of Neuroscience* **10**, 1886–1891.

ROBERTS, A. & CLARKE, J. D. W. (1982). The neuroanatomy of an amphibian embryo spinal cord. *Philosophical Transactions of the Royal Society* B **296**, 195–212.

ROBERTS, A., SOFFE, S. R. & DALE, N. (1986). Spinal interneurons and swimming in frog embryos. In *Neurobiology of Vertebrate Locomotion*, ed. GRILLNER, S., STEIN, P. S. G., STUART, D. G., FORSSBERG, H. & HERMAN, R. M., pp. 279–306. Macmillan, London.

SILLAR, K. T., WEDDERBURN, J. F. S. & SIMMERS, A. J. (1991). The development of swimming rhythmicity in post-embryonic *Xenopus laevis*. *Proceedings of the Royal Society* B **246**, 147–153.

SOFFE, S. R. (1993). Two distinct rhythmic motor patterns are driven by common premotor and motor neurons in a simple vertebrate spinal cord. *Journal of Neuroscience* **13**, 4456–4469.

SPAIN, W. J., SCHWINDT, P. C. & CRILL, W. E. (1991). Two transient potassium currents in layer V pyramidal neurons from cat sensorimotor cortex. *Journal of Physiology* **434**, 591–607.

STORM, J. F. (1988). Temporal integration by a slowly inactivating K^+ current in hippocampal neurons. *Nature* **336**, 379–381.

STORM, J. F. (1990). Potassium currents in hippocampal pyramidal cells. *Progress in Brain Research* **83**, 161–185.

VAN MIER, P., ARMSTRONG, J. & ROBERTS, A. (1989). Development of early swimming in *Xenopus laevis* embryos: myotomal musculature, its innervation and activation. *Neuroscience* **32**, 113–126.

WALL, M. J. & DALE, N. (1994*a*). $GABA_B$ receptors modulate an ω-conotoxin sensitive calcium current which is required for synaptic transmission in the *Xenopus* embryo spinal cord. *Journal of Neuroscience* **14**, 6248–6255.

WALL, M. J. & DALE, N. (1994*b*). A role for potassium currents in the generation of the swimming motor pattern of *Xenopus* embryos. *Journal of Neurophysiology* **72**, 337–348.

WALL, M. J. & DALE, N. (1995). A slowly activating Ca^{2+}-dependent K^+ current that plays a role in termination of swimming in *Xenopus* embryos. *Journal of Physiology* **487**, 557–572.

Acknowledgements

I thank Dr Mark Wall for generously providing some records of the isolated slow K^+ current, Drs Wall and D. Gilday for reading earlier versions of this paper, and the Royal Society and SERC for generous support.

Received 6 December 1994; accepted 24 May 1995.